Impact of Beamforming on Delay Spread in Wideband Millimeter-wave Systems

Berk Akgun[1], Marwan Krunz[1,2], and David Manzi[3]
[1]Department of Electrical and Computer Engineering, University of Arizona, Tucson, AZ
[2]Faculty of Engineering and Information Technology, University of Technology Sydney, Sydney, Australia
[3]Raytheon Corporation, Tucson, AZ
Email: {berkakgun, krunz}@email.arizona.edu, dgmanzi@raytheon.com

***Abstract*—The harsh propagation environment at millimeter-wave (mmW) frequencies can be countered by using large antenna arrays, which can be steered electronically to create directional beams. Knowledge of the key channel characteristics in this environment, including the delay spread, the coherence time, and the coherence bandwidth, plays a significant role in optimal adaptation of the transmission waveform. In this paper, we focus on analyzing the delay spread of a directional mmW channel. A high delay spread causes inter-symbol interference (ISI), which can be mitigated by concatenating cyclic prefixes (CPs) to data symbols at the expense of lower spectral efficiency. Considering a single mmW link, whose transmitter (Tx) and receiver (Rx) are equipped with uniform planar arrays (UPAs), we study the impact of various beamforming attributes (e.g., antenna-array size, beamwidth, beam direction, and beam misalignment) on the average and root-mean-square delay spread. We use detailed simulations with accurate 3GPP channel models and conduct extensive experiments using a 4×8 UPA at 28 GHz to verify our analysis. Based on this analysis, we study the optimal beamforming configuration at the Rx for a given Tx beamformer so as to maximize the spectral efficiency. Our proposed beam selection method finds the best Rx beam direction that results in a low delay spread and high signal-to-noise ratio (SNR). Our extensive simulation and experimental results verify that this method significantly improves the spectral efficiency, almost doubling the data rate in some cases.**

***Index Terms*—Beamforming, millimeter-wave, delay spread, single-carrier modulation, multipath, cyclic prefix.**

I. Introduction

A. Background and Motivation

Millimeter-wave (mmW) spectrum is an integral part of future wireless communications, e.g., 5G and WiGig. Its abundant bandwidth (e.g., about 1.3 GHz in the 28 GHz band, 2.1 GHz in the 39 GHz band, and 14 GHz in the 60 GHz band) promises to address the ever-increasing demand for mobile data [1], [2]. While the channel characteristics have been extensively studied for sub-6 GHz bands, only a few efforts focused on wideband mmW channel modeling and characterization (e.g., [3]–[7]). Efficient and reliable wireless communications of mmW frequencies require knowledge of the channel between the transmitter (Tx) and the receiver (Rx). Such knowledge can be utilized to design robust waveforms that account for channel fluctuations in time and frequency.

In a typical RF environment, multiple copies of the transmitted signal arrive at the Rx through different paths. These multipath components (MPCs) interfere with subsequently transmitted symbols, causing inter-symbol interference (ISI). Significant research has been done on the mitigation of ISI by means of equalization, multicarrier modulation, and spread spectrum techniques [8]. To combat ISI at mmW frequencies, single-carrier modulation methods are generally preferred to multicarrier techniques, such as orthogonal frequency division multiplexing (OFDM) [1], [6], [7]. In particular, OFDM is very sensitive to hardware impairments, including power amplifier (PA) nonlinearity, carrier frequency offset, strong phase noise, and the dynamic range/power of the ADC/DAC. Given the challenges of designing low-cost RF components at mmW frequencies, multicarrier systems face a heavy performance degradation. In [6], [7], the authors showed the effectiveness of single-carrier modulation methods that employ frequency-domain equalization (FDE) in mmW systems (the complexity of FDE is much lower than that of time-domain equalization). WiGig technology also employs single-carrier modulation with four 2.16 GHz channels centered on 58.32, 60.48, 62.64, and 64.8 GHz, respectively [2]. To enable FDE and mitigate ISI in single-carrier systems, cyclic prefix (CP) is inserted before data symbols. The addition of CP, however, reduces the spectral efficiency.

A key aspect of mmW systems is the feasibility of highly directional communications (beamforming). Due to the short wavelength, a large antenna array can be integrated into a small form-factor radio. With proper analog/digital processing of signals fed into these antenna elements, a mmW transmission can be beamed along a specific direction. This beamforming gain compensates for the severe signal attenuation at mmW frequencies. Due to directionality, the Rx captures fewer MPCs compared to omnidirectional communications. This reduces the delay spread, defined as the difference between the time of arrival of the earliest and latest significant MPCs. On the other hand, the narrower the beam the more likely beam misalignment will occur between the Rx and the Tx. This, in turn, reduces the number of captured MPCs at the Rx, which also impacts the delay spread.

In this paper, we analyze the average and root-mean-square (RMS) delay spread in directional (electronically steerable) mmW communications, for the purpose of optimizing waveform design. We study how these metrics are impacted by various beamforming attributes, including antenna size, beamwidth, beam direction, and beam misalignment. First,

we derive the channel autocorrelation function, considering simplified 3GPP channel models. Using this function, we calculate the power delay profile (PDP). We then study the RMS delay spread and its implications on the CP duration. Our main contributions are summarized as follows:

- We analyze the impact of beamforming on the average and RMS delay spread (closed-form expressions are provided), considering uniform planar arrays (UPAs) at both Tx and Rx. In our analysis, we further consider keyhole antenna and simplified 3GPP channel models for analytical tractability. Our results show that the antenna size, beamforming direction, and beam misalignment significantly affect the delay spread. We further show that in certain cases, introducing small beam misalignment can actually help reduce the delay spread.
- For a given Tx beamformer, we determine the optimal beamforming configuration at the Rx so as to maximize the spectral efficiency. Using our delay spread analysis, a method is proposed for selecting the best Rx beam direction that results in low delay spread and that achieves high signal-to-noise ratio (SNR). Note that the delay spread dictates the minimum CP length needed to mitigate ISI. Our beam selection method reflects the effects of both the instantaneous received signal power and the CP overhead.
- We validate our analytical results by conducting extensive simulations based on detailed 3GPP channel models (without any simplifications) and by incorporating UPAs with non-isotropic elements and realistic antenna patterns. Furthermore, we conduct extensive experiments at 28 GHz using a 4×8 UPA and a 20 dBi gain horn antenna. Our simulation and experimental results further verify the effectiveness of our proposed beam selection method. In fact, in certain scenarios, our results indicate that the spectral efficiency of a single-carrier mmW system can be almost doubled by a proper selection of the Rx beam.

B. Related Work

Even though the delay spread has been extensively investigated for sub-6 GHz systems, only a few efforts focused on this issue for mmW systems. In [3] and [4], the authors conducted mmW propagation measurements based on directional horn antennas and presented statistical channel models for wideband mmW systems. They also reported the RMS delay spread values for some specific scenarios. However, their results are limited to horn antennas and do not embrace the unique attributes of UPAs. In contrast to horn antennas, as the beam direction of a UPA varies, the resulting beamwidth and antenna gain also vary. Furthermore, the impacts of the relative angular orientation of a beam and the channel spatial lobe were not considered in these studies. The authors in [5] investigated the performance of narrowband and wideband directional beamformers in terms of improving channel metrics, including RMS delay spread. They showed that a wideband beamformer results in a shorter delay spread than a narrowband beamformer, as the former includes more MPCs. The relation between the delay spread and beamforming attributes was not studied, as we do in our paper. In [9] the authors studied the coherence bandwidth and coherence time in narrowband multiple-input multiple-output (MIMO) systems, considering non-isotropic scattering and directional antenna patterns. Nonetheless, they did not focus on mmW channels and UPAs. Furthermore, the dependence of delay spread on various beamforming parameters was not studied in [9].

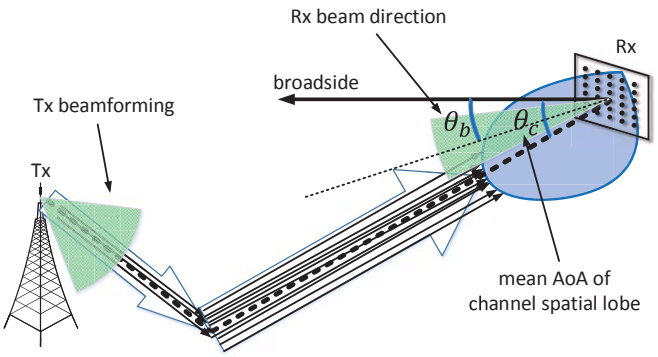

Fig. 1. Target scenario, where the Tx signal reaches the Rx by propagating through multiple paths. The figure shows the Rx angular power distribution within a certain range of angles, called channel spatial lobe. Dashed line represents the middle of the MPCs. Beam misalignment is shown in this example ($\theta_b \neq \theta_c$).

II. System Model

We consider a point-to-point mmW link with electronically steerable UPAs at the Tx and Rx. The targeted scenario is shown in Figure 1, in which a transmitted signal reaches the Rx by propagating through multiple paths. These MPCs are concentrated around a specific angle at the Rx, i.e., the mean angle of arrival (AoA), and they form a *spatial lobe*. Note that the Rx may have multiple angularly separated spatial lobes [10]. In fact, the authors in [11] reported that the expected number of spatial lobes is 1.8 for a 28 GHz operating frequency. However, it was also reported that the angular dispersion of individual channel lobes is usually much larger than the beamwidth. In other words, Tx and Rx beamwidths are much smaller than the angular distance between different spatial lobes. It suffices to assume a single spatial lobe at the Rx.

For a transmitted wideband signal, multipath delay spread impacts signal reception. In particular, a short transmitted pulse of duration T results in a received signal of duration $T + T_{\rm ds}$, where $T_{\rm ds}$ is the multipath delay spread. If $T_{\rm ds} \gg T$, the MPCs of the transmitted signal interfere with subsequently transmitted signals, causing ISI and a large bit error rate (BER). Due to its numerous advantages (see Section I), single-carrier modulation methods with FDE is widely adopted in mmW systems, including WiGig. To enable FDE and mitigate ISI in single-carrier modulation, CP is inserted before data symbols. The addition of this extra field, however, reduces spectral efficiency. In this paper, we analyze the effect of various system parameters, such as Rx beamwidth, beam

direction, beam misalignment, antenna-array size, and the angular spread of MPCs on the multipath delay spread. This analysis is then used to design optimal antenna coefficients at each phase shifter so as to minimize the CP overhead.

Let $h(\tau;t)$ be the channel response at the Rx at time t for a transmitted impulse at time $t-\tau$, i.e., τ is the path delay. In the case of multiple paths between the Tx and Rx, the generated impulse reaches the Rx with various delays, powers, and AoAs. Let P_n, θ_n, and τ_n denote the power, AoA, and delay of the nth MPC, respectively. Then, $h(\tau;t)$ is given by the sum of all $N(t)$ resolvable MPCs at time t:

$$h(\tau;t)=\sum_{n=1}^{N(t)}\sqrt{P_nG(\theta_n|\theta_b)}e^{-j\Phi_n}\delta(\tau-\tau_n) \qquad (1)$$

where $\delta(.)$ is the Dirac delta function. $G(\theta_n|\theta_b)$ is the Rx antenna gain at angle θ_n when the antenna boresight is beamed in the direction θ_b. Throughout this paper, all angles are defined with respect to the broadside direction of the Rx planar antenna array, e.g., if the Rx beam is directed towards the broadside of its array, then $\theta_b=0°$. For simplicity, we focus on a 2D scenario (extension to 3D models is straightforward). Hence, the underlying angles are defined in the horizontal domain. $\Phi_n=2\pi f\tau-2\pi f_Dt\cos(\theta_n)-\phi_n$, where $\phi_n\in[0,2\pi)$ is the random phase of the nth MPC, at time t, $n=1,\cdots,N(t)$. $f_D=\frac{f\nu}{c}$ is the Doppler spread, where f is the carrier frequency, ν is the Rx speed relative to the Tx, and c is the speed of the light.

A statistical characterization of $h(\tau;t)$ is provided by its autocorrelation function, defined as:

$$A_c(\tau_1,\tau_2;t,\Delta t)=\mathbb{E}[h^*(\tau_1;t)h(\tau_2;t+\Delta t)],\quad \Delta t>0 \quad (2)$$

where $h(\tau_1;t)$ and $h(\tau_2;t+\Delta t)$ are the channel responses associated with an MPC of delay τ_1 at time t and an MPC of delay τ_2 at time $t+\Delta t$, respectively. We further assume that the channel is wide sense stationary with uncorrelated scattering (WSSUS), i.e., a channel response associated with an MPC of delay τ_1 is uncorrelated with the one associated with an MPC of delay τ_2, where $\tau_2\neq\tau_1$. Correspondingly, (2) turns into: $\mathbb{E}[h^*(\tau_1;t)h(\tau_2;t+\Delta t)]=\mathbb{E}[h^*(\tau_1)h(\tau_1;\Delta t)]\triangleq A_c(\tau;\Delta t)$. This equation shows that $A_c(\tau;\Delta t)$ is the average power of the channel as a function of τ and Δt.

III. Delay Spread Analysis

One of the most important characteristics of a wideband channel is its delay spread, as it impacts the CP duration needed to mitigate ISI. In this section, we analyze two delay spread parameters, namely, the average and RMS delay spread. Both measures are typically determined via the power delay profile (PDP), $P_c(\tau)$, which is defined by the autocorrelation function $A_c(\tau;\Delta t)$ with Δt set to zero, i.e., $P_c(\tau)\triangleq A_c(\tau;\Delta t=0)$. The PDP basically provides the average signal power of MPCs as a function of their associated delays. These delays are assumed to follow a random exponential distribution, inline with the widely accepted 3GPP model [12] and the research community (e.g., [11]). Accordingly,

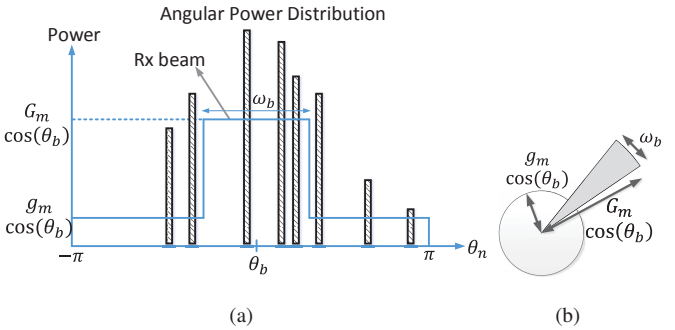

Fig. 2. (a) Antenna and channel models in the Cartesian coordinates. The boresight direction of the Rx beam is θ_b. The figure depicts MPCs with random delays when $\theta_b=\theta_c$. As the difference in θ_c and AoA θ_n of the nth MPC (determined based on its delay τ_n) increases, the power P_n of that path decreases. (b) Keyhole antenna model in polar coordinates.

the PDF of τ_n (the delay of an arbitrary MPC) is given by $f_{\tau_n}(x)=\frac{e^{-x/\hat{\tau}}}{\hat{\tau}}$, where $\hat{\tau}$ is the mean of the random path delay. Consider $P_c(\tau)$:

$$P_c(\tau)=\mathbb{E}[h^*(\tau)h(\tau)]=\mathbb{E}[G(\theta_n|\theta_b)P_n\delta(\tau-\tau_n)]. \qquad (3)$$

The expectation in (3) is over a random variable τ_n. (Note that for a deterministic τ_n, $P_c(\tau)$ has a nonzero value only if $\tau=\tau_n$, meaning that P_c gives the signal power of a path with a delay of τ_n.) P_n and θ_n can be modeled as a function of τ_n [11], [12]. Particularly, following the latest 3GPP channel models and research literature (with some modifications for analytical tractability), we assume that $P_n(\tau_n)=P_Le^{-\tau_n/\hat{\tau}}$, where P_L is a factor that models large-scale channel effects. These effects are common to all MPCs (e.g., they capture path-loss and shadowing degradation). Likewise, we let $\theta_n(\tau_n)=l\kappa\sqrt{\tau_n/\hat{\tau}}+\theta_c$, where θ_c is the mean AoA of the MPCs, κ is the RMS angular spread, and $l\in\{-1,+1\}$ is a uniform random variable. These models can be explained as follows. As the path delay τ_n increases, the power of that path decreases due to higher path loss, reflection, etc. Similarly, its AoA gets farther from the mean AoA, which corresponds to the shortest path (see Figure 2(a)). The parameter l determines whether the AoA of the corresponding path is larger or smaller than the mean AoA. Note that these channel models were obtained via extensive empirical results (see [11], [12]).

For analytical tractability, we also approximate the antenna pattern by a keyhole model, as commonly used in the literature [4], [13] (see Figure 2). More specifically, the antenna gain is modeled as [14]:

$$G(\theta_n|\theta_b)=\begin{cases}G_m\cos(\theta_b), & \text{if}\quad |\theta_b-\theta_n|\leq\frac{\omega_b}{2}\\ g_m\cos(\theta_b), & \text{otherwise}\end{cases} \qquad (4)$$

where ω_b is the beamwidth and G_m is the peak value of main-lobe antenna gain, i.e., $G(\theta_n|\theta_b)=G_m$ when $\theta_b=0$. Similarly, g_m denotes the peak value of side-lobe antenna gain.

Considering (3) and (4), $P_c(\tau)$ is given by:

$$P_c(\tau)=\frac{P_L}{2}\int_{-\infty}^{\infty}\frac{e^{-2\tau_n/\hat{\tau}}}{\hat{\tau}}G\left(-\kappa\sqrt{\frac{\tau_n}{\hat{\tau}}}+\theta_c|\theta_b\right)\delta(\tau-\tau_n)\mathrm{d}\tau_n$$
$$+\frac{P_L}{2}\int_{-\infty}^{\infty}\frac{e^{-2\tau_n/\hat{\tau}}}{\hat{\tau}}G\left(\kappa\sqrt{\frac{\tau_n}{\hat{\tau}}}+\theta_c|\theta_b\right)\delta(\tau-\tau_n)\mathrm{d}\tau_n. \quad (5)$$

The first and the second terms in (5) correspond to the cases when $l=-1$ and $l=1$, respectively. As the two cases occur with the same probability, both terms are divided by two. We refer to the case $\theta_b=\theta_c$, a *perfect beam alignment* at the Rx. However, due to various reasons (e.g., Rx displacement after beam alignment), beam misalignment may occur so that $\theta_b=\theta_c\pm\Delta_\theta$, where Δ_θ denotes the absolute angular value of misalignment. That misalignment impacts the number and PDP of the captured MPCs at the Rx. To take the effect of beam misalignment into account, we let $\Delta_\theta\geq 0$. Combining (4) and (5), we obtain:

$$P_c(\tau)=\begin{cases}\frac{P_L G_m\cos(\theta_b)}{\hat{\tau}}e^{-2\tau/\hat{\tau}}, \text{ if } \Delta_\theta\leq\frac{\omega_b}{2},\ 0\leq\tau<a_1\\ \frac{P_L(G_m+g_m)\cos(\theta_b)}{2\hat{\tau}}e^{-2\tau/\hat{\tau}},\ \text{ if } a_1\leq\tau\leq a_2\\ \frac{P_L g_m\cos(\theta_b)}{\hat{\tau}}e^{-2\tau/\hat{\tau}},\ \text{otherwise}\end{cases}$$

where $a_1\triangleq\hat{\tau}(\omega_b/2-\Delta_\theta)^2/\kappa^2$ and $a_2\triangleq\hat{\tau}(\omega_b/2+\Delta_\theta)^2/\kappa^2$. In the rest of the analysis, we consider two cases: $\Delta_\theta\leq\frac{\omega_b}{2}$ (Case 1) and $\Delta_\theta>\frac{\omega_b}{2}$ (Case 2).

A. Average and RMS Delay Spread

The average delay spread μ_{DS} is defined as:

$$\mu_{\mathrm{DS}}=\frac{\int_0^\infty\tau P_c(\tau)\mathrm{d}\tau}{\int_0^\infty P_c(\tau)\mathrm{d}\tau}. \quad (6)$$

We first calculate the denominator of (6).

Case 1: $\Delta_\theta\leq\frac{\omega_b}{2}$

$$\int_0^\infty P_c(\tau)\mathrm{d}\tau=0.5P_L G_m\cos(\theta_b)$$
$$-0.25P_L(G_m-g_m)\cos(\theta_b)(e^{-2a_1/\hat{\tau}}+e^{-2a_2/\hat{\tau}}).$$

Case 2: $\Delta_\theta>\frac{\omega_b}{2}$

$$\int_0^\infty P_c(\tau)\mathrm{d}\tau=0.25P_L(G_m+g_m)\cos(\theta_b)e^{-2a_1/\hat{\tau}}$$
$$-0.25P_L(G_m-g_m)\cos(\theta_b)e^{-2a_2/\hat{\tau}}.$$

Next, we calculate the numerator of (6).

Case 1: $\Delta_\theta\leq\frac{\omega_b}{2}$

$$\int_0^\infty\tau P_c(\tau)\mathrm{d}\tau=0.25P_L G_m\cos(\theta_b)\hat{\tau}$$
$$-0.25P_L(G_m-g_m)\cos(\theta_b)e^{-2a_1/\hat{\tau}}(a_1+\hat{\tau}/2)$$
$$-0.25P_L(G_m-g_m)\cos(\theta_b)e^{-2a_2/\hat{\tau}}(a_2+\hat{\tau}/2).$$

Case 2: $\Delta_\theta>\frac{\omega_b}{2}$

$$\int_0^\infty\tau P_c(\tau)\mathrm{d}\tau=0.25P_L(G_m+g_m)\cos(\theta_b)e^{-2a_1/\hat{\tau}}(a_1+\hat{\tau}/2)$$
$$-0.25P_L(G_m-g_m)\cos(\theta_b)e^{-2a_2/\hat{\tau}}(a_2+\hat{\tau}/2).$$

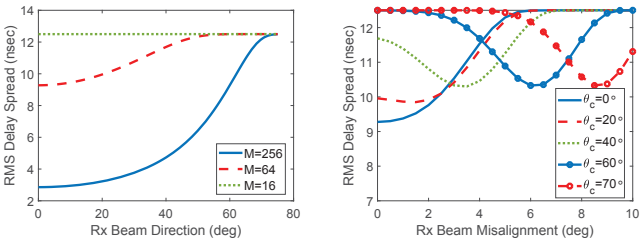

(a) (b)

Fig. 3. RMS delay spread (nsec) vs. (a) Rx beam direction θ_b (deg) under various Rx antenna sizes, (b) Rx beam misalignment Δ_θ (deg) under various θ_c, when $\kappa=5^\circ$ and $\hat{\tau}=25$ nsec.

By plugging the numerator and denominator into (6), we obtain μ_{DS} for Cases 1 and 2.

The RMS delay spread σ_{DS} is defined as:

$$\sigma_{\mathrm{DS}}=\sqrt{\frac{\int_0^\infty\tau^2P_c(\tau)\mathrm{d}\tau}{\int_0^\infty P_c(\tau)\mathrm{d}\tau}-\mu_{\mathrm{DS}}^2}. \quad (7)$$

We already derived the denominator $\int_0^\infty P_c(\tau)\mathrm{d}\tau$ and obtained μ_{DS}. Here, we calculate $\int_0^\infty\tau^2P_c(\tau)\mathrm{d}\tau$ for both cases.

Case 1: $\Delta_\theta\leq\frac{\omega_b}{2}$

$$\int_0^\infty\tau^2P_c(\tau)\mathrm{d}\tau=0.25P_L G_m\cos(\theta_b)\hat{\tau}^2$$
$$-0.25P_L(G_m-g_m)\cos(\theta_b)e^{-2a_1/\hat{\tau}}\left(a_1^2+a_1\hat{\tau}+\hat{\tau}^2/2\right)$$
$$-0.25P_L(G_m-g_m)\cos(\theta_b)e^{-2a_2/\hat{\tau}}\left(a_2^2+a_2\hat{\tau}+\hat{\tau}^2/2\right).$$

Case 2: $\Delta_\theta>\frac{\omega_b}{2}$

$$\int_0^\infty\tau^2A_c(\tau;t)\mathrm{d}\tau=\frac{P_L(G_m+g_m)\cos(\theta_b)}{4}e^{-2a_1/\hat{\tau}}(a_1^2+a_1\hat{\tau}$$
$$+\frac{\hat{\tau}^2}{2})-\frac{P_L(G_m-g_m)\cos(\theta_b)}{4}e^{-2a_2/\hat{\tau}}(a_2^2+a_2\hat{\tau}+\frac{\hat{\tau}^2}{2}).$$

Now that we have derived each term in (7), these terms can be plugged into (7) to obtain σ_{DS}.

B. Numerical Results

To gain insight into the effect of beamforming on the delay spread, the numerical results are provided in this section. We consider that the Rx antenna array is a UPA with half-wavelength antenna separation, and we set ω_b in (4) of our keyhole antenna model to the half-power beamwidth (HPBW) of a UPA in the horizontal domain. Let $M=M_h\times M_v$ denote the total number of antennas in the Rx UPA, where M_h is the number of columns and M_v is the number of antenna elements in each column. Then, if the antenna elements on the UPA are isotropic, the HPBW corresponding to an Rx beam direction θ_b is given by $\omega_b=1.772\left(M_h\cos(\theta_b)\right)^{-1}$ [14]. Note that only the number of columns in the Rx antenna array impacts the beamwidth in the horizontal domain, whereas the total number of antennas impacts the maximum antenna gain G_m. In [14], G_m of an M_v-by-M_h UPA is given by $G_m=\pi M_v M_h$. We also set g_m to the first side-lobe gain of a UPA, which is -13.26 dB relative to G_m [14]. Notice that as P_L terms in

(7) cancel out each other, it does not have an impact on the delay spread.

Figure 3 shows the impact of various parameters on the RMS delay spread $\sigma_{\rm DS}$ when $\kappa = 5^\circ$ and $\hat{\tau} = 25$ nsec (these values are comparable to the ones measured in [3]). In Figure 3(a), we evaluate the effect of Rx beam direction θ_b for different Rx antenna sizes when $\Delta_\theta = 0^\circ$ and $M_v = M_h$. When the Rx UPA is large, $\sigma_{\rm DS}$ increases with θ_b. The main reason is that the beamwidth ω_b gets narrower with smaller θ_b. When ω_b is narrow, the number of MPCs captured at the Rx is small, leading to small $\sigma_{\rm DS}$. Also note that the delay of the MPCs decreases as their AoA gets closer to θ_c. On the other hand, when ω_b is wide enough, $\sigma_{\rm DS}$ converges to a certain point, as all the MPCs are captured. That is also the reason why $\sigma_{\rm DS}$ remains the same for all θ_b values when $M = 16$. Specifically, even the narrowest beam of a 4-by-4 UPA covers all the MPCs. In Figure 3(b), the effect of Rx beam misalignment Δ_θ is investigated for various values of θ_c, when $\theta_b = \theta_c - \Delta_\theta$ and $M = 64$. When Δ_θ increases and θ_c is small, θ_b increases as well. This leads to wider Rx beams, resulting in high delay spread. On the other hand, when θ_c is higher than 20°, the behavior of $\sigma_{\rm DS}$ is different, as seen in Figure 3(b). In particular, as ω_b becomes narrower due to smaller θ_b, $\sigma_{\rm DS}$ decreases with Δ_θ. Furthermore, due to beam misalignment, the Rx beam does not capture the MPCs with higher delays on one side of θ_c. This also contributes to the reduction in $\sigma_{\rm DS}$ compared to the case with $\Delta_\theta = 0^\circ$, where higher-delay and lower-delay MPCs are captured. Hence, $\sigma_{\rm DS}$ takes its lowest value at a certain point. However, as Δ_θ keeps increasing, only the MPCs with higher delays are captured. In other words, the Rx beam does not cover the MPCs with AoAs closer to θ_c. This, in turn, increases $\sigma_{\rm DS}$ for high Δ_θ.

IV. CP Length Optimization

In this section, we aim to design optimal antenna coefficients at the Rx for a given Tx beamforming so as to maximize spectral efficiency. While doing so, the minimum required CP length to overcome ISI is taken into account. To determine the CP duration, we rely on our RMS delay spread analysis. Typically, the CP duration is set in proportion to the RMS delay spread [8], [15]. For example, the authors in [16] reported that a CP whose duration is three times the RMS delay spread provides the optimal system capacity under 3GPP channel models. Let $T_{\rm CP}$ denote the CP duration. We incorporate the CP coefficient, denoted by ρ, such that $T_{\rm CP} = \rho\ \sigma_{\rm DS}$ (e.g., $\rho = 3$ according to [16]). Let B denote the signal bandwidth. Therefore, the useful symbol duration is given by $T_{\rm s} = 1/B$, and the spectral efficiency is reduced to a ratio of $T_{\rm s}/(T_{\rm s} + T_{\rm CP})$ due to the CP.

As shown in Section III, the RMS delay spread is a function of θ_b and Δ_θ. A larger θ_b results in a longer delay spread. Therefore, transmitting towards the beam direction with the highest SNR, i.e., $\theta_b = \theta_c$, may not be optimal if θ_b associated with this beam is large. One may want to exploit another beam direction with smaller θ_b (that will cause a beam misalignment), such that the delay spread is reduced; see Figure 3(b). In this scenario, the shorter CP is needed to mitigate ISI, leading to higher spectral efficiency.

The optimal Rx beam direction is chosen among all available beam directions at the Rx. Let θ_k, $k \in \mathcal{K} \triangleq \{1, \cdots, K\}$, denote these K beam directions. Then, the optimal Rx beam problem is more formally given by:

$$\underset{\{\theta_k,\ k\in\mathcal{K}\}}{\text{maximize}} \left(\frac{T_{\rm s}}{T_{\rm s} + T_{\rm CP}(\theta_k)} \log_2\left(1 + P(\theta_k)\right) \right). \qquad (8)$$

Here, $T_{\rm CP}(\theta_k)$ and $P(\theta_k)$ denote the CP duration and the measured SNR corresponding to the Rx beam direction θ_k, respectively, where $k \in \mathcal{K}$. To solve (8), we propose the following beam-searching scheme. While the Tx is transmitting a known preamble/pilot along a certain beam direction, Rx performs sequential beam sweeping over various θ_k, $\forall k \in \mathcal{K}$. For each θ_k, Rx measures the SNR $P(\theta_k)$. Note that the symbol duration of the transmitted preambles should be long enough to perfectly mitigate the ISI, so that an accurate estimate of $P(\theta_k)$ is obtained at the Rx. By removing the antenna gain effect, which is given in (4), θ_c can be approximated from these measurements, e.g., the Rx beam direction with the highest $P(\theta_k)/G_m \cos(\theta_k)$. Then, by considering both the beam direction and the beam misalignment, the corresponding $T_{\rm CP}(\theta_k)$, $k \in \mathcal{K}$, is computed for a given ρ based on our delay spread analysis. Rx selects the optimal θ_k^* that maximizes (8). In (8), we assume that the addition of the CP perfectly cancels the ISI. Even though our proposed method utilizes this assumption, our simulation results in Section V consider the residual ISI, i.e., we calculate signal-to-interference-plus-noise ratio (SINR) to derive the achievable data rate.

Extension of the proposed scheme to the Tx side is possible via a similar delay spread analysis for the Tx beam. A detailed analysis of this part is left as a future work.

V. Performance Evaluation

A. Simulation Results

In this section, we evaluate the performance of our Rx-beam selection method by comparing it with a benchmark scheme that chooses the Rx beam direction with the highest $P(\theta_k)$, i.e., maximum instantaneous data rate. We conduct extensive simulations to validate our antenna and channel models used in our analytical derivations. Specifically, we implement the 3GPP channel models described in Section 7 of [12]. Urban macro-cell scenarios under line of sight (LoS) conditions are considered where the transmit power is 46 dBm, the operating frequency is 60 GHz, the bandwidth is 100 MHz, and the Tx-Rx distance is 100 m. UPA of half-wavelength antenna spacing and non-isotropic antenna elements (Table 7.3-1 in [12]) are implemented with various numbers of antennas.

In Figure 4(a), the impact of θ_b on $\sigma_{\rm DS}$ is evaluated under various Rx antenna sizes when $\Delta_\theta = 0^\circ$. The results here verify our analytical findings. In other words, both Figures 3(a) and 4(a) show the same effect of θ_b and M on $\sigma_{\rm DS}$. As θ_b increases, $\sigma_{\rm DS}$ also increases due to a wider beamwidth. Similarly, as M increases, narrower beamwidth is obtained, leading to a decrease in $\sigma_{\rm DS}$.

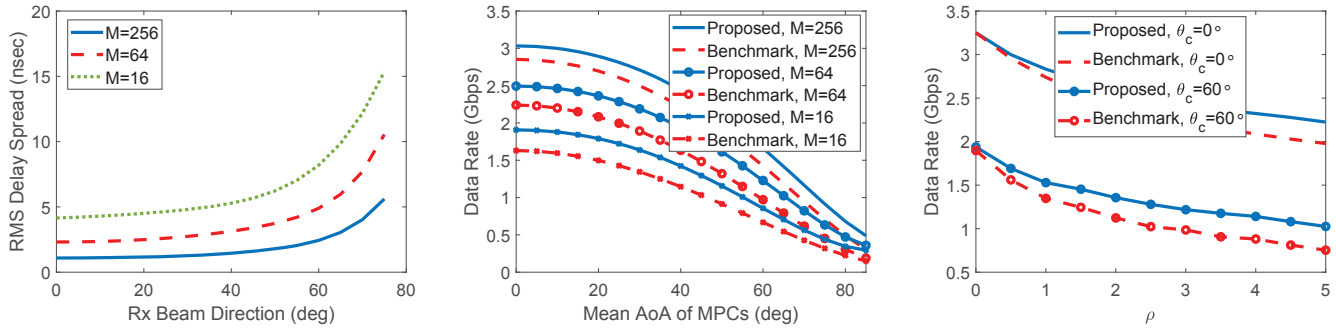

(a) (b) (c)

Fig. 4. Simulation results: (a) RMS delay spread (nsec) vs. θ_b (deg) when $\Delta_\theta = 0°$, (b) data rate vs. θ_c (deg) under various Rx antenna sizes, (c) data rate vs. ρ, when transmit power is 46 dBm, operating frequency is 60 GHz, bandwidth is 100 MHz, and Tx-Rx distance is 100 m.

In Figure 4(b), the impact of θ_c on the data rate is evaluated for various sizes of Rx antenna array when $\rho = 3$. The results indicate that the proposed scheme always outperforms the benchmark. Note that in the benchmark scheme, there is no beam misalignment. On the other hand, a beam misalignment is introduced in our method to reduce the delay spread. This misalignment decreases the instantaneous SNR for the proposed scheme compared to that of the benchmark scheme. However, this loss in SNR is compensated with the shorter CP duration achieved under our method, resulting in a much better spectral efficiency. For example, when $M = 16$ and $\theta_c = 0°$, the data rate is increased by 20% by employing our method. This percentage increases with θ_c, e.g., the proposed and benchmark schemes achieve data rates of 270 Mbps and 140 Mbps, respectively, when $\theta_c = 85°$. In this case, our method almost doubles the data rate of the benchmark. In our results, the lowest gain of the proposed method is observed when $M = 256$ and $\theta_c = 0°$. Even in this case, our method improves the data rate of the benchmark scheme by 7%.

In Figure 4(c), we evaluate the effect of CP coefficient ρ on the data rate for two values of θ_c, when $M = 64$. Recall that $T_{\text{CP}} = \rho\, \sigma_{\text{DS}}$. As expected, both schemes have the same performance when $\rho = 0$, as there is no CP overhead in this case. However, the performance gap between the two schemes increases with ρ, as shown in Figure 4(c).

B. Experiment Results

To verify our analytical and simulation results, we conduct extensive experiments. In the experiment setup (see Figure 5), a 20 dBi gain horn antenna is used at the Tx side to transmit a continuous wave (CW) signal with 0 dBm amplitude at 28 GHz frequency. At the Rx side, a 4×8 UPA is used. Both devices are connected to Keysight N5244B PNA-X Microwave Network Analyzer to generate the CW signal at the Tx and to obtain the received signal power and phase at the Rx. The PNA is connected to a host PC, and the power and the phase results of the received signal are obtained via a TCP connection. The host PC is also connected to the controller of the UPA via USB connection, which enables beamforming by the serial port commands sent from the PC. We conduct

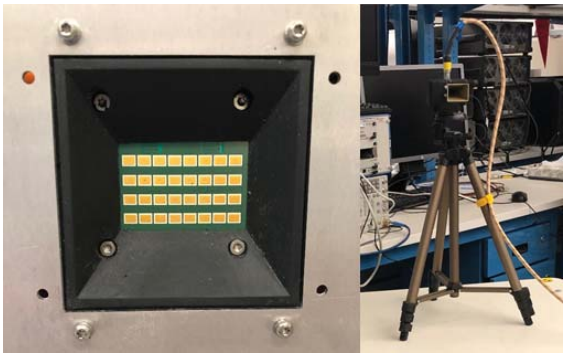

Fig. 5. 4×8 phased array antenna is used at the Rx side (on the panel located at the left) and 20 dBi gain horn antenna is used at the Tx side (on top of a tripod located at the right).

the experiments in an indoor office environment, by moving the Rx away from the Tx where the initial Tx-Rx separation is 3.5 m. The measurements are taken at equally spaced locations such that the LoS angle from the Rx to the Tx changes from $0°$ to $60°$. At each measurement point, the received signal power and phase are recorded for various Rx beam directions. Specifically, as the Tx and Rx antennas were at the same elevation, beam directions were changed only at the azimuthal domain by steering the UPA from $0°$ to $60°$ from broadside with $3°$ steps. Furthermore, for each measurement location and beam direction, the frequency of the CW is swept from 28 GHz to 30 GHz in 5 MHz increments.

From our received signal measurements, we derive the power delay profile, and hence the delay spread corresponding to various beam directions. Figure 6(a) shows the impact of the Rx beam direction on the RMS delay spread when θ_b is set to the LoS direction. It verifies our analytical and simulation results in the sense that as θ_b increases, σ_{DS} increases as well due to wider beamwidths.

In Figure 6(b), we evaluate the effect of the Rx beam misalignment, which is the angle between the LoS direction (i.e., θ_c) and the Rx beam direction. These experiment and the numerical results (obtained via our analysis) in Figure

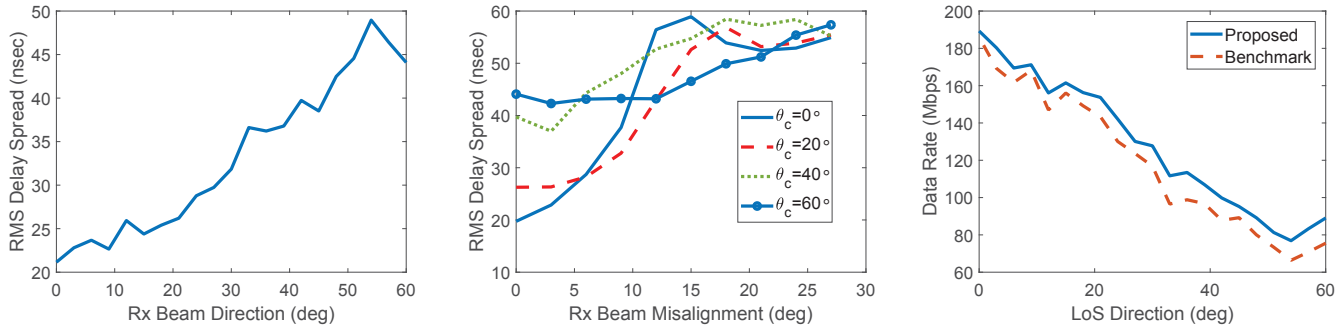

(a) (b) (c)

Fig. 6. Experimental results: (a) RMS delay spread (nsec) vs. θ_b (deg) when $\Delta_\theta = 0°$, (b) RMS delay spread (nsec) vs. Δ_θ (deg) under various LoS directions, (c) data rate vs. LoS direction (deg) between the Tx and the Rx.

3(b) are inline with each other. Figure 6(c) also supports this verification. In particular, we run trace-driven simulations by utilizing our experiments at various frequencies from 28 GHz to 30 GHz to calculate the achievable data rates of our proposed method and the benchmark method. In our proposed method, we use the RMS delay spread values as measured in Figures 6(a) and 6(b), and solve the problem in (8) for various frequencies to calculate the optimal beam direction to be used in a given frequency. Then, the average results are reported in Figure 6(c) for each measurement location. Figure 6(c) shows that our proposed method increases the data rate of the benchmark method by up to 18%.

VI. Conclusions

In this paper, we studied the impact of various beamforming attributes, including antenna size, beamwidth, beam direction, and beam misalignment on RMS delay spread of mmW channels. Simplified 3GPP channel and keyhole antenna models were considered in the analysis with both Tx and Rx being equipped with UPAs. Our results show that the beamforming significantly affects the delay spread. Using our delay spread analysis, we proposed an Rx beam selection method that accounts for both the required length of the CP duration and the achievable SNR. We verified the effectiveness of our proposed method by conducting extensive simulations based on realistic 3GPP channel models. Our results show that the spectral efficiency of a single-carrier mmW system can be significantly increased by a proper selection of the Rx beam.

Acknowledgments

Authors would like to thank Keysight Technologies for providing the experimental setup used in this paper. Authors also would like to thank Irmak Aykin for conducting the experiments. This research was supported in part by NSF and by the Broadband Wireless Access & Applications Center (BWAC). Any opinions, findings, conclusions, or recommendations expressed in this paper are those of the author(s) and do not necessarily reflect the views of NSF.

References

[1] A. Ghosh et al., "Millimeter-wave enhanced local area systems: A high-data-rate approach for future wireless networks," *IEEE J. Sel. Areas Commun.*, vol. 32, no. 6, pp. 1152–1163, June 2014.

[2] IEEE Computer Society, "IEEE Standard-part 11: Wireless LAN medium access control (MAC) and physical layer (PHY) specifications Amendment 3: Enhancements for very high throughput in the 60 GHz band," Dec. 2012. [Online]. Available: https://ieeexplore.ieee.org/document/6392842?tp=&arnumber=6392842.

[3] T. S. Rappaport et al., "Wideband millimeter-wave propagation measurements and channel models for future wireless communication system design," *IEEE Trans. Commun.*, vol. 63, no. 9, pp. 3029–3056, Sep. 2015.

[4] M. K. Samimi and T. S. Rappaport, "3-D millimeter-wave statistical channel model for 5G wireless system design," *IEEE Trans. Microw. Theory Tech.*, vol. 64, no. 7, pp. 2207–2225, July 2016.

[5] S. Wyne et al., "Beamforming effects on measured mm-wave channel characteristics," *IEEE Trans. Wireless Commun.*, vol. 10, no. 11, pp. 3553–3559, Nov. 2011.

[6] H. Nikopour et al., "Single carrier waveform solution for millimeter wave air interface," in *Proc. of the IEEE Globecom Workshops*, Washington, DC, 2016.

[7] S. Buzzi et al., "Single-carrier modulation versus OFDM for millimeter-wave wireless MIMO," *IEEE Trans. Commun.*, vol. 66, no. 3, pp. 1335–1348, March 2018.

[8] A. Goldsmith, *Wireless communications*. Cambridge University Press, 2005.

[9] H. S. Rad and S. Gazor, "The impact of non-isotropic scattering and directional antennas on MIMO multicarrier mobile communication channels," *IEEE Trans. Commun.*, vol. 56, no. 4, pp. 642–652, April 2008.

[10] I. Aykin and M. Krunz, "Fastlink: An efficient initial access protocol for millimeter wave systems," in *Proc. of the ACM MSWiM 2018 Conference*, Montreal, Canada, Oct. 2018, pp. 109–117.

[11] M. R. Akdeniz et al., "Millimeter wave channel modeling and cellular capacity evaluation," *IEEE J. Sel. Areas Commun.*, vol. 32, no. 6, pp. 1164–1179, June 2014.

[12] 3GPP, "Study on channel model for frequency spectrum above 6 GHz," 3GPP, Tech. Rep. TR 38.900 v15.0.0, June 2018.

[13] I. Aykin, B. Akgun, and M. Krunz, "Smartlink: Exploiting channel clustering effects for reliable millimeter wave communications," in *Proc. of the IEEE INFOCOM 2019 Conference*, Paris, France, April 2019, pp. 1117–1125.

[14] R. S. Elliot, *Antenna theory and design*. John Wiley & Sons, 2006.

[15] F. Pancaldi et al., "Single-carrier frequency domain equalization," *IEEE Signal Process. Mag.*, vol. 25, no. 5, pp. 37–56, Sep. 2008.

[16] A. A. Al-jzari, I. Kostanic, and K. H. M. Mabrok, "Effect of variable cyclic prefix length on OFDM system performance over different wireless channel models," *Universal Journal of Communications and Network*, vol. 3, no. 1, pp. 7–14, Feb. 2015.